Korean J. Chem. Eng., 33(2), 688-696 (2016)
DOI: 10.1007/s11814-015-0178-8

pISSN: 0256-1115
eISSN: 1975-7220

Characteristics of $LiFePO_4$/C composite prepared by sonochemical method under multibubble sonoluminescence

Ki-Moon Kang, Hyo-Won Kim, and Ho-Young Kwak†

Mechanical Engineering Department, Chung-Ang University, Seoul 06911, Korea
(*Received 8 May 2015 • accepted 19 August 2015*)

Abstract−$LiFePO_4$/C composites with various weight percent of carbon nanotubes (CNT) were prepared through one-pot sonochemical method under the condition of multibubble sonoluminescence (MBSL). The electrical performance of the composites depends crucially on ultrasound irradiation time, the calcination temperature and duration and weight percent of CNTs. The best initial discharge capacity was obtained for a calcination temperature of 650 °C for 6 h, 30 minutes ultrasound irradiation and with 2 wt% of CNTs. The electric conductivity of the $LiFePO_4$/C composite with 2 wt% CNTs was approximately $3.4 \cdot 10^{-4}$ S/cm. The coin cell made of $LiFePO_4$/C composite whose average diameter is 683 nm exhibits an initial discharge capacity of 142 mAh/g at 0.1 C, a flat and long voltage plateau and low ΔV between the initial charge and discharge plateaus of 0.03 V and small fade rate of capacity of 0.08% per cycle at 0.5 C. The first efficiency, the ratio of the initial discharge to the initial charge capacity, of the $LiFePO_4$/C composite, is about 90%.

Keywords: Lithium Iron Phosphate, Multibubble Sonoluminescence, Carbon Nanotube, Initial Discharge Capacity, First Efficiency, Cathode Material

INTRODUCTION

Lithium iron phosphates ($LiFePO_4$) with an olivine-type structure [1] are promising cathode materials due to their high theoretical capacity of 170 mAh/g [2], cycling stability with a flat discharge plateau [3] and low toxicity [4]. Many works have been devoted to synthesizing $LiFePO_4$ by various synthetic methods, such as solid state reactions [2,5], carbothermal reduction [6,7] microwave processing [8,9] hydrothermal methods [10,11], sol-gel processing [12], and precipitation methods [13,14]. $LiFePO_4$ powders are synthesized by several methods, and their XRD patterns have been compared with theoretical ones [15]. In their study, parasitic peaks in the XRD patterns were absent when the material was synthesized through hydrothermal routes and mechanochemical activation. Various synthetic procedures for the olivine-type $LiFePO_4$ were reviewed in detail by Jugovic and Uskokovic [16], who suggest that hydrothermal synthesis will become a commercially viable approach to the production of this material. The best discharge capacity of 162 mAh/g was obtained at 0.1 C for nano-crystalline $LiFePO_4$ particles synthesized by spontaneous precipitation [13]. However, the initial discharge capacity of bare $LiFePO_4$ powders synthesized by solid-state reaction [5] or microwave processing [9] is less than 120 mAh/g.

As is well known, $LiFePO_4$ particles, which have very poor electric conductivity [2,17] and low lithium-ion diffusion coefficients [1,18], produce a low discharge capacity, high polarization and poor rate capability. To overcome such problems, one prepared smaller $LiFePO_4$ particles [19,20] to increase the diffusion coefficient of the ions. Diverse synthetic methods such as sol-gel process [20,21], solid-state reaction [22,23], co-precipitation [24], carbothermal reduction [25,26], microwave processing [27], hydrothermal stripping [28], hydrothermal synthesis coupled with cupric ion doping [29] and combustion synthesis [30] have been employed to synthesize $LiFePO_4$ composites by various carbon sources to increase the electric conductivity. Dual inorganic/organic carbon sources [31] and dual grapheme/carbon [32] have also been used in the synthesis of $LiFePO_4$/C composites to improve the conductivity of the material. Indeed, nano-sized and carbon-coated $LiFePO_4$ particles deliver a discharge capacity of 150-163 mAh/g at 0.1 C [20,22]. In comparison, $LiFePO_4$ and $LiFePO_4$/C synthesized by solid-state reaction deliver initial discharges of 119 and 158 mAh/g at 0.2 C, respectively [5]. The nano-scale (30-80 nm) $LiFePO_4$/C composites synthesized by co-precipitation deliver a discharge capacity of 155 mAh/g at 0.1 C, while the composites of 80-200 nm in diameter show a lower discharge capacity of 120 mAh/g at the same rate [33]. Polarization, which is related to the difference between the initial charge and discharge plateaus, was also found to be increased with increasing particle size [34].

Although the nano-scale $LiFePO_4$/C composite materials show quite good electrochemical performance, the tap density and energy density decrease as the carbon content increases, which indicates that the carbon content must be kept to a minimum [15]. Furthermore, it is difficult to avoid the degradation of the discharge capacity of nano-sized $LiFePO_4$ materials because of their low crystallization degree upon long-time cycling [35] and relatively low volumetric energy density resulting from the low nanoparticles packing density [36]. Recently, hierarchically structured composites based on porous $LiFePO_4$ with multiwalled carbon nanotubes, which yielded

†To whom correspondence should be addressed.
E-mail: kwakhy@cau.ac.kr

a high tap density, were synthesized [37]. The synthesized composites offered a discharge capacity of 169.6 mAh/g, which is close to the theoretical capability.

Depending on the synthetic method, processing route and environment as well as the starting materials used, the $LiFePO_4$ or $LiFePO_4$/C powders exhibit different size distributions and morphologies [38,39] and thus different electrochemical performances [15,16,31]. The development of new cost-effective and environmentally friendly synthesis routes for industrial production of the materials is still required. Recently, nano-sized $LiFePO_4$ particles were synthesized in supercritical water [40].

Sonochemistry is the application of sonoluminescence (SL), which is a light emission phenomenon associated with the catastrophic collapse of gaseous micro bubbles oscillating under an ultrasonic field [41]. The intense local heating and high pressure inside the bubbles as well as the liquid adjacent the bubble wall induced by this collapse [42] can give rise to unusual effects in chemical reactions. Shock waves form collapsing bubbles in liquid-solid solution, which produces high-velocity inter-particle collisions. A few tens of thousands of transient bubbles generated by the irradiation of high intensity ultrasound in aqueous solution collapse simultaneously to produce blue light under multibubble sonoluminescence (MBSL) conditions [43,44]. Sonochemical processing, especially under the MBSL conditions, has proven to be useful for creating novel materials with unusual properties more rapidly than any other synthetic methods without producing any harmful materials [45,46]. Recently, supported Ni catalysts with a core/shell structure showing good conversion efficiency and thermal stability in various methane reforming conversions were also synthesized under the MBSL conditions [47,48].

In this study, homogeneous $LiFePO_4$ composites with various wt% of CNTs (carbon nanotubes) were prepared through a one-pot sonochemical method under the MBSL conditions. The optimal parameters of ultrasound irradiation time, calcination temperature and duration and wt% of the carbon used to produce the $LiFePO_4$/C composites under the MBSL conditions were determined. The physical properties and electrochemical performances including the first efficiency of the prepared materials were tested and measured.

EXPERIMENTAL

1. General Procedures

A detailed description of the experimental apparatus of MBSL has been reported elsewhere [43]. The sonochemical reaction system consists of a cylindrical quartz cell into which a 5 mm-diameter titanium horn (Misonix XL 2020, USA) is inserted. It was operated at 20 kHz and 220 W, which is quite intense compared to other typical ultrasound irradiation processes and kept at 1.4 atm with argon gas. The solution inside the cell was kept at approximately 25 °C by a circulating water bath, which was found to be an optimal temperature for synthesizing nano materials.

2. Synthesis of $LiFePO_4$/C

The detailed procedure for preparing $LiFePO_4$ powder is shown in Fig. 1. The $LiFeSO_4$ powders were prepared using phosphoric acid (H_3PO_4, Sigma Aldrich, 85%) as a phosphate source, iron sulfate heptahydrate ($FeSO_4 \cdot 7H_2O$, Fluka, 99%) as an iron source, and lithium hydroxide monohydrate ($LiOH \cdot H_2O$, Sigma Aldrich, 98%) as a lithium source. The same starting materials were used to synthesize $LiFePO_4$ via a hydrothermal route [10,11].

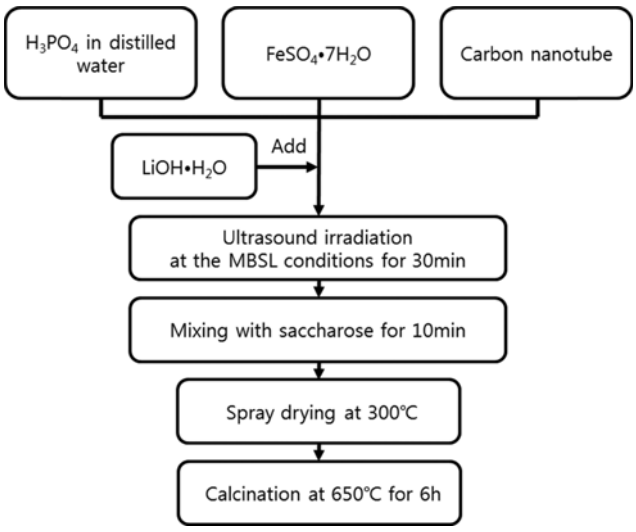

Fig. 1. Procedure for synthesizing $LiFePO_4$/C by a sonochemical method under MBSL conditions. H_3PO_4, $FeSO_4 \cdot 7H_2O$ and $LiOH \cdot H_2O$ were mixed in a molar ratio of 1 : 1 : 1.

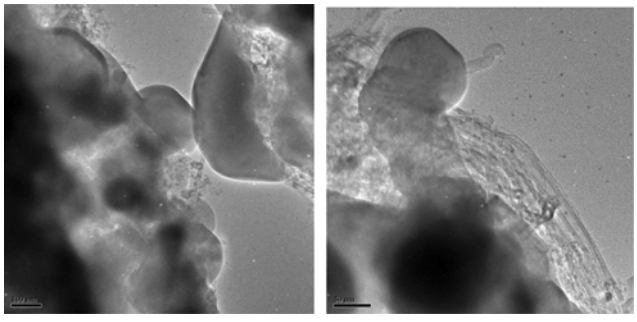

Fig. 2. TEM images of $LiFePO_4$/C particles covered partially by CNTs.

First, $FeSO_4 \cdot 7H_2O$ was dissolved completely in H_3PO_4 solution to avoid the formation of Fe(OH) and mixed with various weight percent (1-6 wt%) of CNTs. Next, $LiOH \cdot H_2O$ was added to the mixture. Some $LiFePO_4$ particles are partly covered by CNTs through such mixing process, as shown in Fig. 2. The molar ratio of Li : Fe : P was 1 : 1 : 1, and a typical mole number of $FeSO_4$ was 0.2 M in 1 L of water. Ultrasound irradiation was applied to the mixture under the MBSL conditions for 10-60 min while the solution temperature was maintained at 25 °C. After mixing the solution with saccharose for 10 min, the resultant material was sprayed into a dryer at 300 °C. The amorphous powder synthesized under the MBSL conditions was subsequently calcined at an appropriate temperature (550-800 °C) for 6 h in argon atmosphere, producing $LiFePO_4$/C crystalline composites.

3. Optimization Procedure to Prepare $LiFePO_4$/C

Various combinations of $FeSO_4$ mole number (0.05 to 0.5 M in 1 L of water), duration of ultrasound irradiation under MBSL conditions (10 to 60 min), calcination temperature of $LiFePO_4$ pow-

der (550 to 800 °C) and the weight percent of CNTs (1 to 6 wt%) were applied to identify the conditions that maximized the initial discharge capacity (mAh/g) and minimized the difference between the charge and discharge voltage ΔV for $LiFePO_4$/C. From a series of preliminary studies, the optimal parameters for the ultrasound irradiation time (30 min), calcination temperature (650 °C) and duration (6 h) and the wt% of CNTs (2 wt%) were found. Based on these optimal parameters, the optimization procedures to synthesize $LiFePO_4$/C were repeated, as follows.

Various mole numbers of phosphoric acid (H_3PO_4) from 0.1 M to 0.5 M in 1 L of water with a fixed ultrasound irradiation time of 30 min, calcination temperature of 650 °C and 2 wt% of CNTs were tested to find the best electrochemical performance of $LiFePO_4$/C.

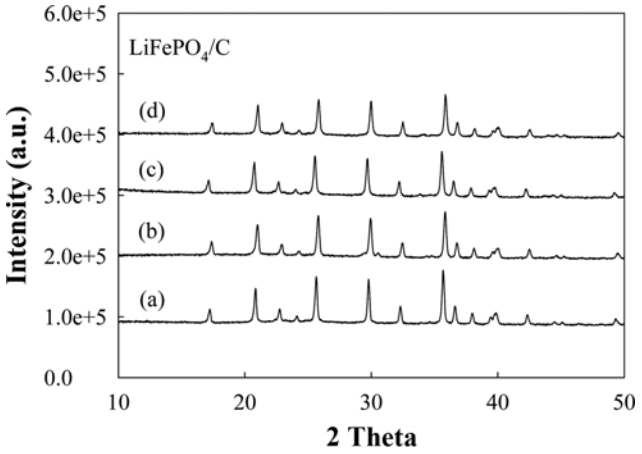

Fig. 3. XRD patterns for $LiFePO_4$/C prepared with various mole numbers of H_3PO_4 in 1 L of water: 0.1 M, (b) 0.2 M, (c) 0.3 M and (d) 0.5 M.

In this trial, similar XRD patterns showing the characteristics of $LiFePO_4$ were obtained for all mole numbers of H_3PO_4, as displayed in Fig. 3. However, the average particle size of the $LiFePO_4$/C powder increased as the mole number of H_3PO_4 in 1 L of water increased. The best electrochemical performance in terms of initial charge capacity and a low value between charge and discharge plateaus, ΔV of 0.03 V was obtained using 0.2 M H_3PO_4 in 1 L of water, as confirmed in Table 1, even though the first efficiency with 0.2 M of H_3PO_4 was lower compared to the one with higher mole of H_3PO_4. The first efficiency, which is defined as the ratio of the initial discharge capacity to the charge capacity, is a very important parameter for better battery efficiency.

With a fixed mole number of 0.2 M H_3PO_4 in 1 L of water, a calcination temperature of 650 °C for 6 h and 2 wt% CNTs, the ultrasound irradiation time under the MBSL conditions was varied from 10 to 60 min. Among the trials, 30 min of ultrasound radiation provided the best electrochemical performance, as shown in Table 2.

The calcination of $LiFePO_4$/C powder should proceed because the material prepared by the sonochemical method under MBSL conditions is amorphous due to the high cooling rate, which exceeds 10^8 K/s [49]. As shown in Table 3, the calcination of the $LiFePO_4$/C powders at 650 °C for 6 h with a fixed ultrasound irradiation time of 30 min, 0.2 M H_3PO_4 in 1 L of water and 2 wt% of CNTs provides the best electrical performance. In contrast, the powder was reduced to $Li_3Fe_2(PO_4)_3$ after calcination at 800 °C for 6 h. The $Li_3Fe_2(PO_4)_3$ powder delivers the lowest initial discharge capacity as well as the first efficiency.

Carbon nanotubes and carbon black were used to improve the conductivity of the $LiFePO_4$ by mixing the carbon source directly rather than mixing citric acid [20], glucose [25] or lauric acid [50]. In these trials, an ultrasound irradiation time of 30 min, calcination temperature of 650 °C, 0.2 M H_3PO_4 in 1 L of water were used.

Table 1. Voltage plateau, value between charge and discharge plateaus, initial discharge capacity, the first efficiency and average size of $LiFePO_4$/C depending on moles of phosphoric acid (H_3PO_4) in 1 L of water. Irradiation time of ultrasound under MBSL conditions is fixed as 30 min and the same mole number of $FeSO_4 \cdot 7H_2O$ and $LiOH \cdot H_2O$ was used in this reaction

Mole number of phosphoric acid in 1 L of water	Voltage plateau (V)		ΔV (V)	Initial discharge capacity at 0.1 C (mAh/g)/ First efficiency (%)	Average size of $LiFePO_4$/C (nm)
	Charge	Discharge			
0.05	3.46	3.39	0.07	109.4/98.2	240
0.1	3.53	3.37	0.16	142.9/92.4	374
0.2	3.45	3.42	0.03	142.2/92.5	683
0.3	3.46	3.42	0.04	137.4/94.0	2037
0.5	3.49	3.39	0.10	135.2/94.7	5129

Table 2. Voltage plateau, value between charge and discharge plateaus and initial discharge capacity depending ultrasound irradiation time for $LiFePO_4$/C

Irradiation time (min)	Voltage plateau (V)		ΔV (V)	Initial discharge capacity at 0.1 C (mAh/g)
	Charge	Discharge		
10	3.48	3.40	0.08	89.4
20	3.47	3.42	0.05	132.6
30	3.45	3.42	0.03	142.2
40	3.48	3.43	0.05	141.3
60	3.50	3.41	0.09	137.2

Table 3. Voltage plateau, value between charge and discharge plateaus, initial discharge capacity and the first efficiency of $LiFePO_4$/C depending on calcination temperatures

Temperature (°C)	Voltage plateau (V)		ΔV (V)	Initial discharge capacity at 0.1 C (mAh/g)/ First efficiency (%)
	Charge	Discharge		
550	3.46	3.41	0.05	138.1/6.5
600	3.47	3.36	0.11	141.7/94.1
650	3.45	3.42	0.03	142.3/92.5
700	3.50	3.35	0.15	142.2/91.4
750	3.52	3.39	0.13	125.5/87.4
800	3.53	3.35	0.18	28.2/21.6

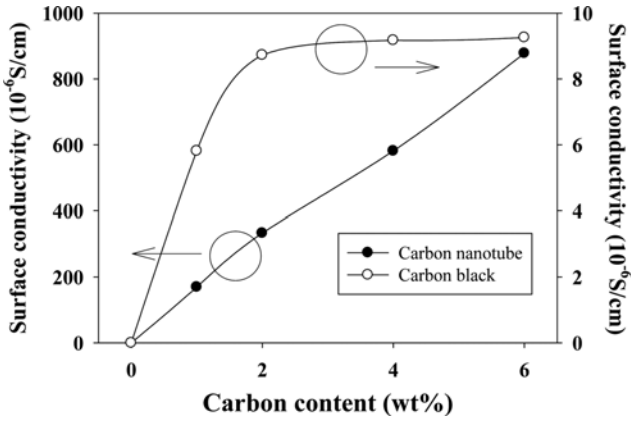

Fig. 4. Surface conductivity of $LiFePO_4$/C composites depending on the content of the carbon source.

The electric conductivity of the $LiFePO_4$-carbon black composites plateaued at $8.7 \cdot 10^{-6}$ S/cm for the 2 wt% of the carbon black, as shown in Fig. 4. On the other hand, the electric conductivity of the $LiFePO_4$-CNT composites increased linearly with the wt% of the CNTs. However, the best electrochemical performance was achieved for 2 wt% of CNTs for $LiFePO_4$/C composites yielding an electric conductivity of $3.3 \cdot 10^{-4}$ S/cm even though the 6 wt% of CNT composites had a higher electric conductivity of $8.8 \cdot 10^{-4}$ S/cm. This observation indicates that the electrochemical properties of $LiFePO_4$ can be improved by increasing the electric conductivity to a certain extent. For both composites with CNTs and carbon black, the best in the first efficiency occurred at 4 wt% of carbon content. For the $LiFePO_4$/C core/shell nano-composites fabricated using $FePO_4$/polyaniline [51], the best electrochemical performance was obtained with 8.6 wt% of carbon. Further increases in the carbon shell thickness led to a decrease in the discharge capacity of the material. The best discharge capacity for $LiFePO_4$ composites with 2 wt% carbon black was 127.5 mAh/g. The discharge capacity obtained with $LiFePO_4$ composites with carbon black is comparable to the discharge value obtained by Zhang et al. [52]. On the other hand, Sun et al. [53] obtained similar initial discharge capacity of 160 mAh/g at 0.1 C both from $LiFePO_4$ composite with CNTs and carbon black. In addition, the discharge capacity obtained with the bare $LiFePO_4$ in our study is only approximately 93.2 mAh/g, which is similar to that obtained with commercial $LiFePO_4$ powder [54].

In summary, as seen in Tables 1, 2, 3 and 4, the best initial discharge capacity of 142.2 mAh/g and lowest value between charge and discharge plateaus, ΔV of 0.03 V were obtained with 0.2 M $FeSO_4$ in 1 L of water, 30 min of ultrasound irradiation time, calcination at 650 °C for 6 h and 2 wt% of CNTs, which can be considered an optimized case in this particular study. The $LiFePO_4$ composite with 2 wt% of CNTs synthesized at these conditions is designated as $LiFePO_4/C_{op}$.

4. Characterization of $LiFePO_4/C_{op}$

Structural analysis was carried out using a powder X-ray diffractometer (MiniflexII, Rigaku, Japan). The diffraction patterns were collected for scattering angles ranging from 10° to 80° with a

Table 4. Voltage plateau, polarization between charge and discharge plateaus, initial discharge capacity and the first efficiency of $LiFePO_4$/C depending on the contents of carbon sources

Carbon source	Contents (wt%)	Voltage plateau (V)		ΔV (V)	Initial discharge capacity at 0.1 C (mAh/g)/ First efficiency (%)
		Charge	Discharge		
	0	3.56	3.40	0.16	93.2
Carbon nanotubes	1	3.47	3.40	0.07	118.2/90.2
	2	3.45	3.42	0.03	142.2/90.2
	4	3.48	3.39	0.09	131.5/96.5
	6	3.47	3.35	0.12	127.1/89.6
Carbon black	1	3.48	3.40	0.08	112.2/68.2
	2	3.47	3.41	0.06	127.5/87.3
	4	3.47	3.40	0.07	111.8/94.2
	6	3.48	3.39	0.09	105.4/----

time step of 4°/min using a Cu Kα radiation source (λ=1.5406). The morphology of the $LiFePO_4$/C composite was observed with a high-resolution transmission electron microscope (HR-TEM: JEM-3010, JOEL, Japan) and a field emission scanning electron microscope (FE-SEM: JSM-6700F). The surface elemental analysis was conducted using energy dispersion X-ray (EDX) analysis. The particle size distribution was measured by a dynamic light-scattering particle size analyzer (Malvern Zetasizer Nano). The conductivity was measured by a four-point probe (Keithley 2400, USA). The carbon content in $LiFePO_4$/C was measured by weighing the dried residue of a known amount of $LiFePO_4$/C dissolved in hydrochloride acid (Junsei, Japan).

5. Electrochemical Performance of $LiFePO_4/C_{op}$

The performance of the $LiFePO_4$/C as a cathode was evaluated using a coin-type cell with a lithium metal anode. The cathode was prepared by mixing 75 wt% $LiFePO_4/C_{op}$ composites with 17.5 wt% carbon black and 7.5 wt% polyvinylidine fluoride (PVDF) in n-methyl-2-pyrrolidone (NMP) solution. Lithium metal (Sigma Aldrich 99.99%) was used as the anode, and a 1 M $LiPF_6$ in an ethylene carbonate/diethyl carbonate (EC/DMC) (1 : 1 vol%) mixture was used as the electrolyte with a Celgard membrane as the separator. The initial charge and discharge of the coin cells were measured at 0.1 C between 2.5 and 4.4 V. The coin cells were cycled at 0.5 C between 2.5 and 4.4 V in an automatic battery cycler (WBCS 300, WonA Tech, Korea).

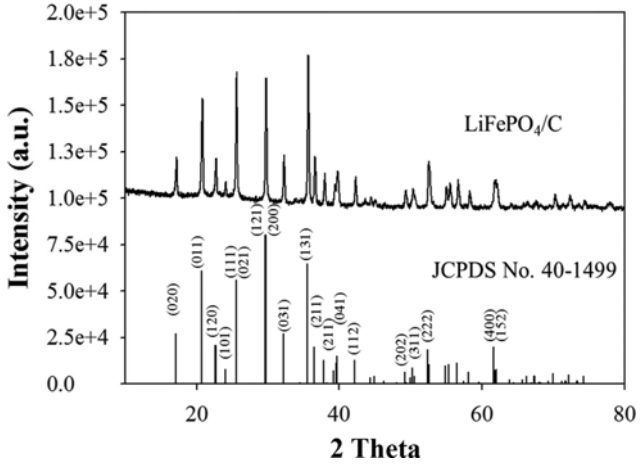

Fig. 5. Comparison of the XRD pattern between 0.2 M $LiFePO_4/C_{op}$ shown in Fig. 2 and the reference data (JCPDS NO. 40-1499).

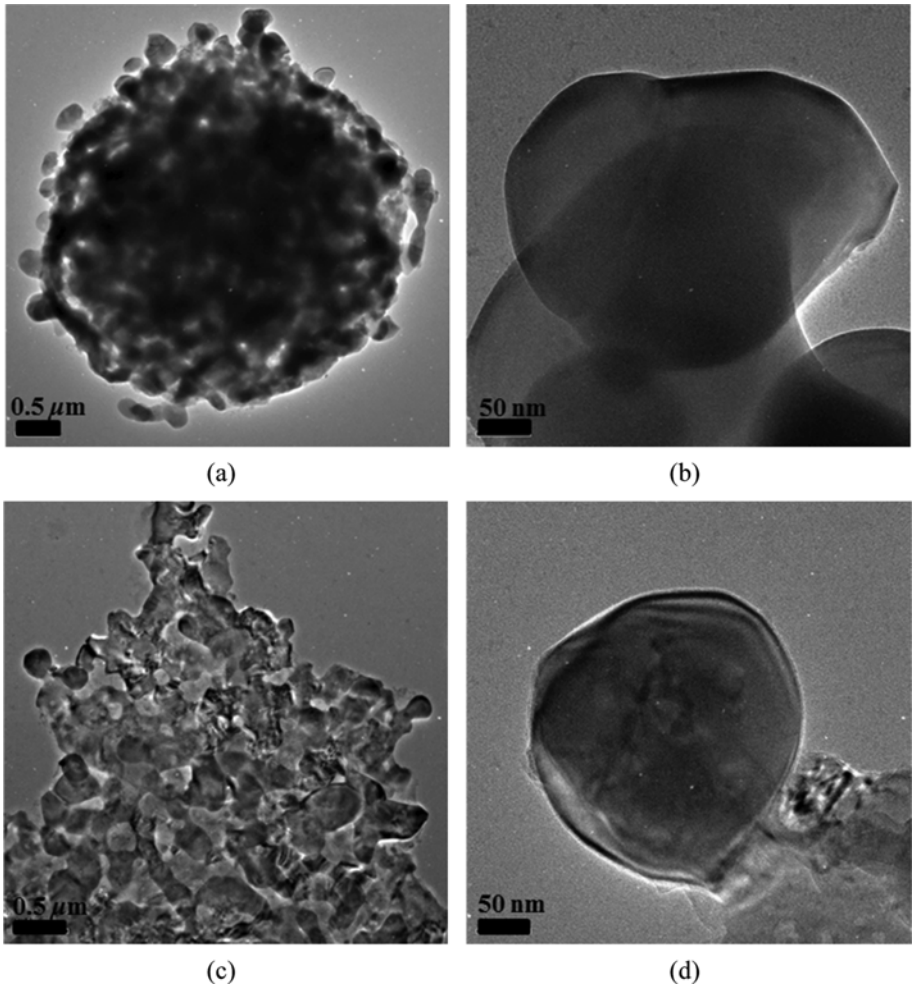

Fig. 6. HR-TEM images of $LiFePO_4/C_{op}$: (a) and (b) before calcination; (c) and (d) after calcination at 650 °C.

RESULTS AND DISCUSSION

1. Structure of $LiFePO_4/C_{op}$

The XRD patterns of the $LiFePO_4/C$ synthesized under the optimized conditions and the reference data for JCPDS No. 40-1499 are shown in Fig. 5. The peaks of the plots in Fig. 5 can be completely matched to the reference data for olivine $LiFePO_4$ with an orthorhombic lattice (Pnma), despite the difference in the relative magnitudes of the peaks at 2θ=21.0°, 25.81°, 29.43° and 35.84° and the reference data. However, our measured data for the XRD patterns, including the relative magnitude of the peaks, are in exact correspondence with the theoretical patterns for $LiFePO_4$ [15]. No parasitic peaks due to impurities such as Fe(II) and Fe(III) [15] are observed in Fig. 5.

2. Morphology of $LiFePO_4/C_{op}$

Figs. 6(a) and 6(b) show the HR-TEM images of the $LiFePO_4/C_{op}$ powder synthesized under the optimized conditions before calcination, while Figs. 6(c) and 6(d) show the corresponding images for the powder after calcination at 650 °C for 6 h. The size of the individual particles is approximately 250-300 nm, as seen from Figs. 6(b) and 6(d). The particle size distribution of the $LiFePO_4/C_{op}$ with an average size of 682 nm is shown in Fig. 7(a). After 24 h ball milling, the average size of the powder whose size distribution is shown in Fig. 7(b) decreased to 496 nm. After spray drying and calcina-

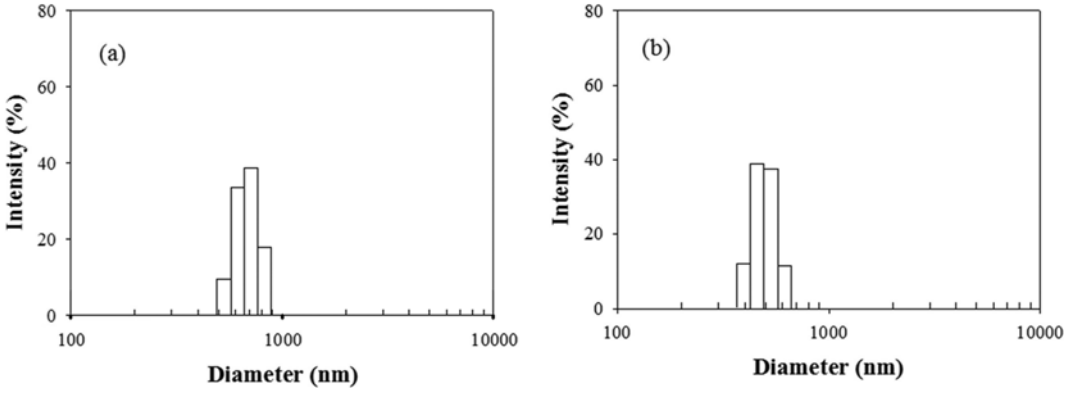

Fig. 7. Particle size distributions of $LiFePO_4/C_{op}$ (a) without and (b)with 24 h of ball milling.

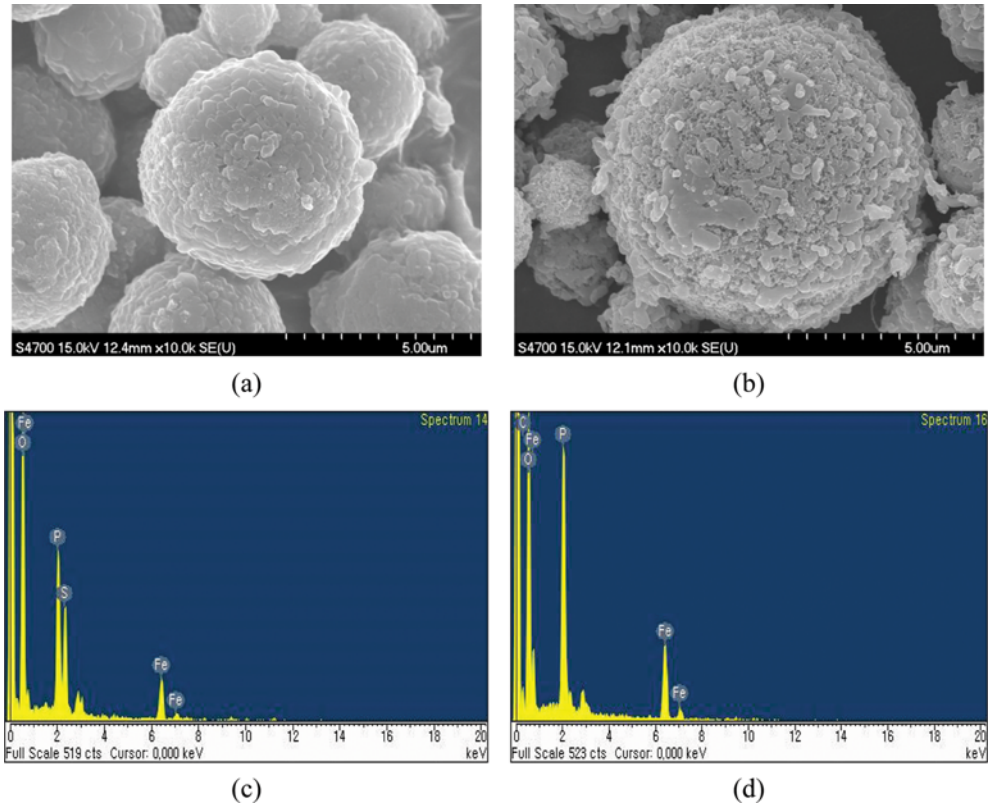

Fig. 8. FE-SEM images and EDX of $LiFePO_4/C_{op}$ after spray drying: (a) and (c) before calcination: (b) and (d) after calcination at 650 °C.

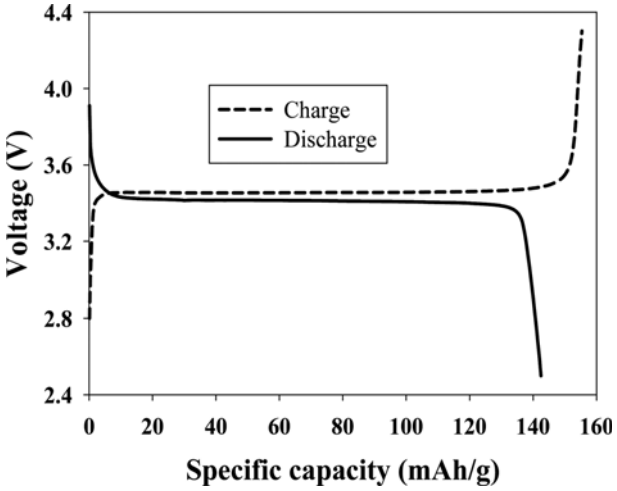

Fig. 9. Initial charge-discharge profile at a current rate of 0.1 C for $LiFePO_4/C_{op}$.

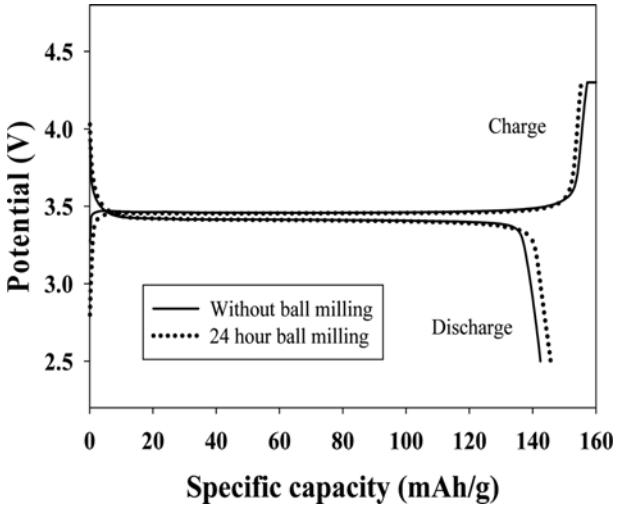

Fig. 11. Initial charge-discharge profile at a current rate of 0.1 C for $LiFePO_4/C_{op}$ with or without ball milling.

tion, the particle size reaches several micrometers, as shown in the FE-SEM images (Fig. 8). Such micro-size particles are appropriate for preparing the coin cells for the electrochemical test. The calcination process is needed because impurities such as sulfur can be removed through this process, as confirmed from the EDX profiles shown in Fig. 8.

3. Electrochemical Characteristics of $LiFePO_4/C_{op}$

Fig. 9 shows the initial charge/discharge curves of $LiFePO_4/C_{op}$ synthesized under the optimal conditions at 0.1 C. The sample exhibits a long discharge voltage plateau at 3.40 V, which indicates that the two-phase redox reaction proceeds via a first-order transition between $LiFePO_4$ and $FePO_4$ [20]. Earlier voltage drop in the initial discharge plateau [12,13,32,33,35,51,52] is not seen in Fig. 9. The initial discharge capacity and the first efficiency for $LiFePO_4/C$ are 142 mAh/g, and 90%, respectively. Similar initial discharge capacity (145.3 mAh/g) at 0.1 C and the first efficiency (90%) were obtained from $LiFePO_4/C$ nanoparticles (200 nm) synthesized by a hydrothermal process [38]. Although the discharge capacity measured in this study is much lower than the value obtained from the carbon nanotube-embedded $LiFePO_4$ [55], the discharge capacity of 142 mAh/g is 52% higher than that obtained from bare $LiFePO_4$ powder as shown in Fig. 10. The small voltage difference between the charge and discharge plateaus of about 0.03 V is evidence of this excellent kinetics.

As seen in Table 1, particles larger than 2 μm in diameter produced lower initial discharge capacity than those with 683 nm in diameter, even though the first efficiency increased slightly for larger particles. On the other hand, the small particles comprising the $LiFePO_4/C_{op}$ (496 nm) composites obtained via 24 h ball milling produced a better initial discharge capacity of 145.7 mAh/g, as shown in Fig. 11. Furthermore, the first efficiency increased to 95% after ball milling. In fact, the commercial $LiFePO_4/C$ particles, whose diameter decreased to 232 nm after 18 h ball milling, achieved an initial discharge capacity of 161 mAh/g at 0.1 C during the first five cycles and 130.4 mAh/g at 0.5 C after 10 cycles [34]. Smaller particles may have contributed to the increase the ion diffusion, improv-

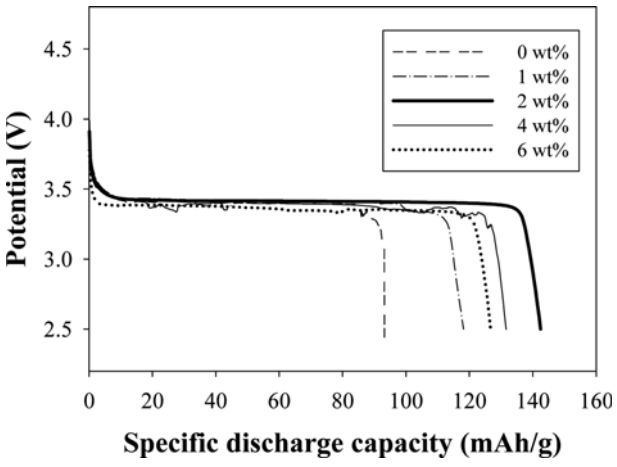

Fig. 10. Specific discharge capacity of $LiFePO_4/C$ depending on weight % of of carbon nanotube.

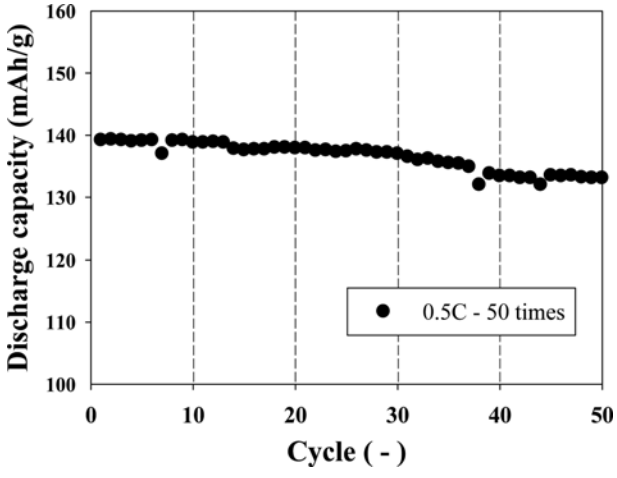

Fig. 12. Cycling performance of $LiFePO_4/C_{op}$ at a 0.5 C in the voltage range of 2.5 to 4.4 V.

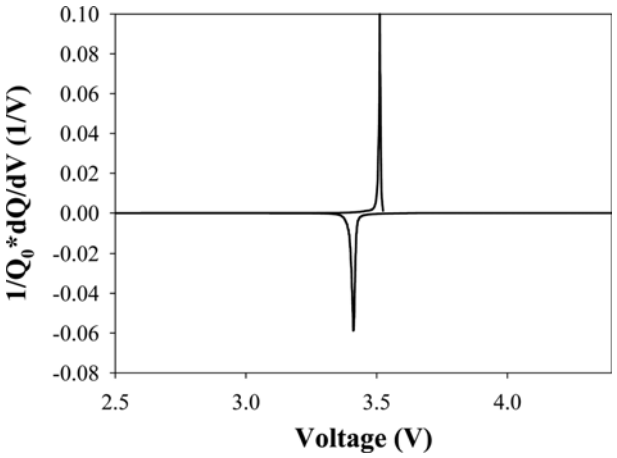

Fig. 13. dQ/dV plot of $LiFePO_4/C_{op}$ obtained from the charge-discharge profile in the voltage range of 2.5 to 4.4 V.

ing the electrochemical reaction [1,18].

The cycle life of the $LiFePO_4/C_{op}$ composites at 0.5 C to a cut-off voltage between 2.5-4.4 V is shown in Fig. 12. After 50 cycles, the discharge capacity of the sample decreased to 133 mAh/g; thus the capacity decreased by approximately 0.08% per cycle.

The dQ/dV versus potential plot [56] obtained from the charge-discharge profile of the 0.2 M $LiFePO_4/C_{op}$ half-cell cycled at 0.5 C is shown in Fig. 13. This plot provides the potential of lithium de-insertion and insertion. The charge peak shows that the lithium ion de-insertion occurs at 3.483 V, and the discharge peak shows the lithium ion insertion occurs at 3.410 V. At 0.5 C, the charge process ends at 3.528 V, and the discharge process ends at 3.359 V. No noticeable side reaction was observed in the 2.5-4.5 V potential range tested in this study.

CONCLUSIONS

A $LiFePO_4$-carbon nanotube composite for the cathode material was prepared through a one-pot sonochemical method under MBSL conditions, providing a new synthesis method for specialty materials to reduce energy consumption and processing time. This composite with carbon nanotubes (CNTs) proved to be very effective in enhancing the electronic conductivity of $LiFePO_4$. The prepared $LiFePO_4$/C composites with 2 wt% of CNTs achieved a charge capacity of 142 mAh/g at 0.1 C, which is much higher than the value of 93.2 mAh/g for bare $LiFePO_4$ powder. The composite shows a long voltage plateau, a small difference between the initial charge and discharge voltage of 0.03 V, a low capacity fade rate of 0.08% per cycle at 0.5 C and the first efficiency of 90%.

ACKNOWLEDGEMENTS

This work was supported by the Seoul R&D program (10543).

REFERENCES

1. A. K. Padhi, K. S. Nanjundaswamy and J. B. Goodenough, *J. Electrochem. Soc.*, **144**, 1188 (1997).
2. A. K. Padhi, K. S. Nanjundaswamy, C. Masquelier, S. Okada and J. B. Goodenough, *J. Electrochem. Soc.*, **144**, 1609 (1997).
3. A. Yamada, S. C. Chung and K. Hinikuma, *J. Electrochem. Soc.*, **148**, A224 (2001).
4. F. Sauvage, E. Baudrin, L. Gengembre and J. M. Tarascon, *Solid State Ionics*, **176**, 1869 (2005).
5. K. Yang, Z. Deng and J. Suo, *J. Power Sources*, **201**, 274 (2012).
6. B. Q. Zhu, X. H. Li, Z. X. Wang and H. J. Guo, *Mater. Chem. Phys.*, **98**, 373 (2006).
7. C. W. Kim, J. S. Park and K. S. Lee, *J. Power Sources*, **163**, 144 (2006).
8. M. Higuchi, K. Katayama, Y. Azuma, M. Yukawa and M. Suhara, *J. Power Sources*, **119-121**, 258 (2003).
9. L.Wang, Y. Huang, R. Jiang and D. Jia, *Electrochim. Acta*, **52**, 6778 (2007).
10. J. Chen and M. S. Whittingham, *Electocchem. Commun.*, **8**, 855 (2006).
11. G. Meligrana, C. Gerbaldi, A. Tuel, S. Bodoardo and N. Penazzi, *J. Power Sources*, **160**, 516 (2006).
12. J.-K. Kim, J.-W. Choi, G. S. Chauhan, J.-H. Ahn, G.-C. Hwang, J.-B. Choi and H.-J. Ahn, *Electrochim. Acta*, **53**, 8258 (2008).
13. P. P. Prosini, M. Carewska, S. Scaccia, P. Wisniewski, S. Passerini and M. Pasquali, *J. Electrochem. Soc.*, **149**, A886 (2002).
14. G. Arnold, J. Garche, R. Hemmer, S. Strobele, C. Volger and M. Wohlfahrt-Mehrens, *J. Power Sources*, **119-121**, 247 (2003).
15. S. Franger, F. L. Cras, C. Bourbon and H. Ronault, *J. Power Sources*, **119-121**, 252 (2003).
16. D. Jugovic and D. Uskokovic, *J. Power Sources*, **190**, 538 (2009).
17. P. S. Subramanya, B. Ellis, N. Coombs and L. F. Nazar, *Nature Mater.*, **3**, 147 (2004).
18. D. Y. W. Yu, C. Fietzek, W. Weydanz, K. Donoue, T. Inoue, H. Kurokawa and S. Fujitani, *J. Electrochem. Soc.*, **154**, A253 (2007).
19. L. Wang, W. Sun, X. Tang, X. Huang, X. He, J. Li, Q. Zhang, J. Gao, G. Tian and S. Fan, *J. Power Sources*, **244**. 94 (2013).
20. K.-F. Hsu, S.-Y. Tsay and B.-J. Hwang, *J. Mater. Chem.*, **14**, 2690 (2004).
21. Y. Lin, J. Wu and W. Chen, *Ionics*, **19**, 227 (2013).
22. X. Yan, G. Yang, J. Lin, Y. Ge, H. Xie, X. Pan and R. Wang, *Electrochim. Acta*, **54**, 5770 (2009).
23. F. Cheng, W. Wan, Z. Tan, Y. Huang, H. Zhou, J. Chen and X. Zhang, *Electrochim. Acta*, **56**, 2999 (2011).
24. D. Jugovic, M. Mitric, M. Kuzmanovic, N. Cvjeticanin, S. Skapin, B. Cekic, V. Ivanovski and D. Uskokovic, *J. Power Sources*, **196**, 4613 (2011).
25. L. Wang, G. C. Liang, X. Q. Ou, X. K. Zhi, J. P. Zhang and J. Y. Cui, *J. Power Sources*, **189**, 423 (2009).
26. F. Yu, J. Zhang, Y. Yang and G. Song, *Electrochim. Acta*, **54**, 7389 (2009).
27. M. S. Song, Y.-M. Kang, J.-H. Kim, H.-S. Kim, D.-Y. Kim, H.-S. Kwon and J.-Y. Lee, *J. Power Sources*, **166**, 260 (2007).
28. C. Miao, P. Bai, Q. Jiang, S. Sun and X. Wang, *J. Power Sources*, **246**, 232 (2014).
29. B. Pei, Q. Wang, W. Zhang, Z. Yang and M. Chen, *Electrochim. Acta*, **56**, 5667 (2011).
30. N. Kalaiselvi and A. Manthiram, *J. Power Sources*, **195**, 2894 (2010).
31. Q.-B. Liu, S.-J. Liao, H.-Y. Song and Z.-X. Liang, *J. Power Sources*, **211**, 52 (2012).

32. C. Su, X. Bu, L. Xu, J. Liu and C. Zhang, *Electrochim. Acta*, **64**, 190 (2012).
33. S. Wang, H. Yang, L. Feng, S. Sun, Y. Yang and H. Wei, *J. Power Sources*, **233**, 43 (2013).
34. G. T. K. Fey, Y. G. Chen and H. M. Kao, *J. Power Sources*, **189**, 169 (2009).
35. Y. Wang, Y. Wang, E. Hosono, K. Wang and H. Zhou, *Angew. Chem. Int. Ed.*, **47**, 7461 (2008).
36. Y.-G. Guo, J.-S. Hu and L.-J. Wan, *Adv. Mater.*, **20**, 2878 (2008).
37. G. Qin, Q. Ma and C. Wang, *Electrochim. Acta*, **115**, 407 (2014).
38. B. Pei, H. Yao, W. Zhang and Z. Yang, *J. Power Sources*, **220**, 317 (2012).
39. Q. Wang, W. Zhang, Z. Yang, S. Weng and Z Jin, *J. Power Sources*, **196**, 10176 (2011).
40. S.-A. Hong, S. J. Kim, K. Y. Chung, Y.-W. Lee, J. Kim and B.-I. Song, *Chem. Eng. J.*, **229**, 313 (2013).
41. F. R. Young, *Sonoluminescence*, CRC Press, New York (2005).
42. E. B. Flint and K. S. Suslick, *Science*, **253**, 1397 (1991).
43. K. Byun and H. Kwak, *J. Photochem. Photobiology A-Chem.*, **175**, 45 (2005).
44. I. Ko and H. Kwak, *J. Phys. Soc. Jap.*, **79**, 1224401 (2010).
45. C. H. Hwang, J. Park, M. Song, J. H. Lee and I. W. Shim, *Bull. Korean Chem. Soc.*, **32**, 2207 (2011).
46. J. Wang, W. Guo, S. Liu and D. Li. *Ultrasonic Sonochem.*, **19**, 464 (2012).
47. H. W. Kim, K. M. Kang and H. Kwak. *Int. J. Hydrogen Energy*, **34**, 3351 (2009).
48. H.-W. Kim, K.-M. Kang, H. Kwak and J. H. Kim, *Chem. Eng. J.*, **168**, 775 (2011).
49. K. S. Suslick, *Science*, **247**, 1439 (1990).
50. D. Choi and P. N. Kumta, *J. Power Sources*, **153**, 1064 (2007).
51. Z. Jiang and Z.-J. Jiang, *J. Alloys Compd.*, **537**, 308 (2012).
52. S. S. Zhang, J. L. Allen, K. Xu and T. R. Jow, *J. Power Sources*, **147**, 234 (2005).
53. X. Sun, J. Li, C. Shi, Z. Wang, E. Liu, C. He, X. Du and N. Zhao, *J. Power Sources*, **220**, 264 (2012).
54. H. Liu, Q. Cao, L. J. Fu, C. Li, Y. P. Wu and H. Q. Wu, *Electrochim. Commun.*, **8**, 1553 (2006).
55. J.-P. Jegal and K.-B. Kim, *J. Power Sources*, **243**, 859 (2013).
56. H. Zehng, L. Chai, X. Song and V. Battaglia, *Electrochim. Acta*, **62**, 256 (2012).